Journal of Materials Chemistry A

PAPER

View Article Online
View Journal | View Issue

Cite this: J. Mater. Chem. A, 2016, 4, 3082

Optimized immobilization of ZnO:Co electrocatalysts realizes 5% efficiency in photo-assisted splitting of water†

Anahita Azarpira,*[a] Johannes Pfrommer,[b] Katarzyna Olech,[a] Christian Höhn,[a] Matthias Driess,[b] Bernd Stannowski,[c] Thomas Schedel-Niedrig[a] and Michael Lublow*[ad]

Organic solvents with varied electrophoretic mobility have been employed for deposition of nanocrystalline ZnO:Co particles onto fluorinated tin oxide supports. Evaluation of the electrochemical activity for the oxygen evolution reaction proves a clear solvent-dependence with highest activity upon deposition from acetonitrile and lowest activity upon deposition from ethanol. Analysis of the resulting layer thickness and density attributes the improved electrochemical activity of acetonitrile-prepared samples to larger film thicknesses with lower film densities, *i.e.* to films with higher porosity. The findings suggest that the ZnO:Co films represent an initially nanocrystalline system where the catalytic activity is predominantly confined to a thin surface region rather than to comprise the entire volume. Closer inspection of this surface region proves successive *in operando* transformation of the nanocrystalline to an amorphous phase during evolution of oxygen. Furthermore, less active but highly transparent ZnO:Co phases, prepared from ethanol-containing suspensions, can be successfully employed in a stacking configuration with a low-cost triple-junction solar cell. Thereby, a solar-to-hydrogen efficiency of 5.0% in splitting of water at pH 14 could be realized. In contrast, highly light-absorbing acetonitrile/acetone-prepared samples limit the efficiency to about 1%, demonstrating thus the decisive influence of the used organic solvent upon electrophoretic deposition. Stability investigations over several days finally prove that the modular architecture, applied here, represents an attractive approach for coupling of highly active electrocatalysts with efficient photovoltaic devices.

Received 13th September 2015
Accepted 5th December 2015

DOI: 10.1039/c5ta07329d

www.rsc.org/MaterialsA

Introduction

Producing clean fuels from sustainable resources is one of the main challenges for research and industry in the twenty-first century due to imminent environmental and political demands. Hydrogen (H_2) represents a very attractive, emission-free alternative fuel because of its large energy density (143 kJ g^{-1}) and is therefore a very promising candidate to substitute fossil energy resources. There are various routes for the production of hydrogen. Among them, photoelectrochemical splitting of water is of particular importance since it benefits from the abundant supply of energy by solar irradiation. In order to produce hydrogen by water splitting, water must be dissociated into its constituent parts, molecular hydrogen (two-electron process) and oxygen (four-electron process). Due to the slower kinetics of the oxygen evolution reaction (OER), this half-cell reaction is recognized[1–6] as the bottleneck for efficient overall splitting of water. The OER reaction therefore requires, in general, higher overpotentials with respect to the thermodynamic potential (+1.23 V *vs.* NHE at pH0) than the corresponding hydrogen evolution reaction (HER). These overpotentials lead to partial loss of energy and reduce the overall efficiency of the water splitting reaction.[7–9] Suitable electrocatalysts are therefore required to reduce the energy loss, and they should, for economic reasons, be developed from earth-abundant source-materials. These materials may generate light-induced charge carriers on their own, as bismuth vanadate[10] and hematite[11] or may be employed on photoactive supports, as nickel oxide on silicon,[12] for instance. Particularly by use of electrocatalysts which are not responsive to illumination (*e.g.* NiO, IrO_2, RuO_2), the development of efficient photoelectrode architectures is facilitated: these materials permit individual testing of the catalytic activity in the dark, *i.e.* independently on light-absorption behavior and photon-to-charge-carrier transformation. Subsequently, electrocatalysts which combine most effectively electrochemical activity and

[a]Helmholtz-Zentrum Berlin für Materialien und Energie GmbH, Institute for Solar Fuels, Berlin, Germany. E-mail: lublow@helmholtz-berlin.de
[b]Technical University, Department of Chemistry, Berlin, Germany
[c]Helmholtz-Zentrum Berlin für Materialien und Energie, PVcomB, Berlin, Germany
[d]Albert-Ludwigs-Universität, Department of Chemistry, Freiburg, Germany

† Electronic supplementary information (ESI) available. See DOI: 10.1039/c5ta07329d

beneficial optical properties can be immobilized on photoactive supports. Already many efforts have been done by Trasatti and Lodi to realize efficient evolution of oxygen in acidic electrolytes employing IrO_2 and RuO_2.[13] Although these catalysts are very efficient for the OER, the use of expensive iridium and ruthenium makes large-scale application cost-ineffective. Recent work on metastable cobaltoxidic materials by Shao-Horn *et al.* showed the great potential of employing intrinsically metastable materials (*e.g.* $LiCoO_2$) for the *in situ* formation of amorphous, cobaltoxidic water oxidation catalysts (WOC).[14–16] Pfrommer and coworkers have shown that Co-substituted ZnO (ZnO:Co) is an efficient precatalyst[17] and leads to higher hole-conductivity in the *in situ* formed WOC nanocomposite, due to the formation of core shell structures with the polar ZnO:Co precatalyst integrated in the film.[18] For activity assessment and application as WOC, pre-synthesized catalyst powders require a suitable immobilization method in order to functionalize the catalysts on appropriate semiconductors. In the case of ZnO:Co, electrophoretic deposition (EPD) from powder suspension in acetone onto fluorinated tin oxide (FTO) supports has been successfully employed to fabricate electrodes with stable activity at pH7 and pH12.[17] EPD represents a cost-effective technology for realization of colloidal coatings in many fields of application.[19,20] Generally, powder materials are suspended in a chemically inert solvent and are transported under the influence of a direct-current electric field towards the supporting electrode.[19–23] The key parameter in EPD is the velocity of the particles which determines the deposition rate and is dependent on the physical properties of the solvent. In the case of ZnO:Co, the influence of varied organic solvent on the properties of the resulting electrodes has not yet been sufficiently explored. Likewise, optimized preparation conditions for application of ZnO:Co films also in photo-assisted evolution of oxygen have not been identified. Particularly the latter subject can help transferring efficient electrocatalysts to the important field of photoelectrolytic splitting of water.

In this work, we provide fundamental insight into the role of the organic solvent upon electrophoretic deposition of electrocatalytically active ZnO:Co and correlate structural, electrochemical as well as optical properties to the applied preparation procedure. It will be shown, firstly, that the organic solvent considerably influences the size of the active surface area of the deposited films. It is thereby possible to identify acetonitrile as organic solvent which provides higher activity than the reported acetone solution. Secondly and most important, ethanol will be identified as promising solvent for the deposition of ZnO:Co onto photo-active semiconductor supports. Although with ethanol the observed onset potentials are lowest, optical transparency is highest. Consequently, it can be shown that is thereby possible to improve light-incoupling into a triple-junction solar cell which helps overcompensating the lower activity of the electrocatalytic layer. The resulting modular combination of the photovoltaic device with the top ZnO:Co/FTO electrode realizes 5.0% solar-to-hydrogen efficiency. Strong light absorption by acetonitrile- and acetone-prepared samples, on the other hand, limits the corresponding efficiency to about 1%.

Experimental

ZnO:Co film preparation

ZnO:Co nanoparticles were synthesized by solvolysis of a heterobimetallic (Co, Zn) single source precursor (SSP) mixture composed of tetranuclear cubanodic clusters of the di-2-pyridylmethandiolato (dpdH) ligand[24,25] (see ESI Fig. S1†). The solvolytic reaction commenced in benzylamine at low temperature (180 °C) for 10 minutes.[17] The green powder of ZnO:Co has an average crystal size of 17.2 nm, 42.2% cobalt content and 47.3 $m^2\,g^{-1}$ surface area. 6 mg of the powder were suspended in 12 ml organic solvent; 1 mg of iodine was added to the solution in order to induce a positive surface charge at the particles and to invoke an electric-field-induced transport to the cathode. The solution was stirred in an ultrasonic bath for 5 min. Subsequently EPD was carried out at a potential of −10 V for 4, 7 and 10 min, respectively, at room temperature. Film deposition was observed only at the negatively polarized electrode (the support). In our EPD cell, two fluoride tin oxide electrodes were used in a two-electrode arrangement, *i.e.* without reference electrode. The two electrodes of area size 1.25 × 2.5 cm^2 each were fixed at a mutual distance of 0.5 cm in a glass beaker of 15 ml capacity. For electric connection, an InGa eutectic was spread at the upper part of the FTO and connected with clips to the external power source. The deposition cell was protected against the ambient by a Teflon cap with two rectangular slits into which the FTO electrodes were inserted. Preparation conditions were kept constants for all investigated solvents, *i.e.* ethanol, acetone and acetonitrile.

Solar-cell supports

Triple-junction amorphous/microcrystalline silicon solar cells (a-Si:H/a-Si:H/μc-Si:H) were employed for investigation of photo-assisted water splitting in alkaline electrolytes (pH 14). The used solar cells were fabricated by PVcomB (Berlin-Adlershof, Germany) and are characterized by two a-Si:H and one μc-Si p–i–n junctions with absorber layer thicknesses of 70, 320 and 700 nm, respectively. Fabrication details are similar to those given in the work of Kirner *et al.*[26] For optimized protection of the solar cell and assessment of the light-absorbing behavior of the respective ZnO:Co films, the ZnO:Co/FTO samples were positioned on the front-side of the solar cells, *i.e.* at the glass-protected photoactive side of the solar cell. Electrical contact was realized by a wire connecting the solar cell and the electrocatalytic layer. Thereby, the solar cell was not exposed to the electrolyte and the modular architecture allowed for simple exchange of used ZnO:Co/FTO top-junctions. This arrangement takes into account the superior life-time of solar cell devices in comparison to any currently available protection scheme for photoelectrodes under anodic electrochemical conditions. Moreover, efficiency calculations were simplified since the incident light was simultaneously illuminating the electrocatalytic film and the underlying solar cell, *i.e.* the size of the illuminated area in the denominator of the efficiency equation (eqn (3)) corresponds to the total area of the electrode.

Sample analysis

The deposited films were investigated by X-ray diffraction (XRD) in Bragg–Brentano geometry, using a Bruker AXS (D8 Advance) diffractometer. A Cu K_α X-ray source was used with a wavelength of 1.5406 Angström. In order to achieve high resolution and an excellent signal to noise ratio, the X-ray beam was directed towards the sample *via* a Göbel mirror. For detection of the diffracted radiation, a SOL-X energy dispersive detector was employed. The measured diffraction patterns were analyzed with the software EVA3. X-ray photoelectron spectroscopy (XPS) was carried out with Al K_α excitation at an ESCA system supplied by Specs, Germany. Optical measurements of ZnO:Co films, deposited on FTO substrates, were performed using a Perkin Elmer Lambda 950 UV/VIS spectrometer. Modulated surface photovoltage (SPV) measurements were done in fixed capacitor mode[27] to determine the defect-related absorption edge of the deposited films. The samples were illuminated using a quartz prism monochromator equipped with halogen lamp in the photon energy range 0.4–3.8 eV. The light from the monochromator was chopped at a frequency of 8 Hz, and the SPV signal was detected with a double-phase lock-in-amplifier (EG & G, 7260 DSP). The morphology of the semiconductor was investigated by scanning electron microscopy (SEM) using a LEO Gemini 1530 from Zeiss, Germany, and a Thermo Fisher EDX system. The thickness of the samples was determined with a Veeco-Dektak 8 stylus profilometer. Electrochemical measurements were performed using a biologic potentiostat in three-electrode configuration with Pt counter electrode and a Ag/AgCl reference electrode (+205 mV *vs.* RHE). Simultaneously, the potential difference between working and counter electrode was monitored. Oxygen evolution at the working electrode and evolution of hydrogen at the Pt-counter electrode took place in a single compartment, *i.e.* without use of a membrane. Two steel clips were connected to the surface of the sample as front contacts. For individual testing of the ZnO:Co layers on FTO in the dark, the geometrical surface area of the working electrode, exposed to the electrolyte, was 0.5 cm^2. For testing of the combined system with silicon solar cell, a larger working area of 1.5 cm^{-2} was used. Thereby, the full photoactive area of the underlying solar cell (1 cm × 1 cm) could be illuminated. The solar cell characteristics were initially measured using a solar simulator. At the photoelectrochemical setup, a W-I light source from Dolan Jenner was used. The light intensity of the light source was adjusted such that an equivalent solar cell behavior was realized during photoelectrochemical measurements, yielding about 100 mW cm^{-2} illumination intensity. Differential electron mass spectroscopy (DEMS)[28,29] was carried out to detect the produced gases during cyclic voltammetry. The inlet system between the electrochemical cell and the differentially pumped vacuum system of the mass spectrometer (Balzers; QMI 420, QME 125, QMA 125 with 901 off axis SEM) consisted of a porous hydrophobic membrane, covered by a 100 nm thick Au-layer. The ZnO:Co working electrode was attached to this layer. Oxygen which is formed in an electrochemical experiment at the ZnO:Co working electrode diffuses thereby partly into the mass spectrometer and is monitored simultaneously with the electrochemical data. DEMS data are therefore of qualitative nature only and do not allow deducing the Faradaic efficiency. All DEMS experiments were carried out in N_2-purged 0.5 M KOH at scan rates of 2 mV s^{-1}. Due to the specifics of the DEMS setup diffusion-related additional overpotentials are present and have to be attributed to the small spacing between the sample and the used membrane.

Results and discussion

In Fig. 1a, the effect of the organic solvent on the film thickness (left axis) and the density of the layers (right axis) is summarized for varied deposition times. Thicknesses of the layers were measured by a DEKTAK profilometer and the density of the layers was calculated by measuring the deposited mass. In total, nine samples were prepared by suspending ZnO:Co electrocatalysts in ethanol, acetone and acetonitrile. Electrophoretic deposition was carried out for 4, 7 and 10 min each. As shown in Fig. 1a, the resulting layer thickness is lowest for ethanol and highest for acetonitrile for each deposition time. The inverse dependence is observed for the calculated density. In general, the deposition rate is observed to be constant, *i.e.* the layer thickness increases linearly with time. The visual appearance of the samples after 10 min is depicted as inset in Fig. 1b.

An obvious color variation from dark green after deposition from acetonitrile to light green after deposition from ethanol is observed. This difference in color is attributed to a corresponding variation of the film thickness (see Fig. 1a). Moreover, the variation of the calculated density of the layers proves an increasing porosity with deposition time. This finding is particularly important for electrocatalytic processes where an increased active surface area is crucial for an enhanced electrochemical activity. This observed trend implies that under the applied deposition potential smallest particles reach the substrate first, forming thereby a compact layer, while bigger particles are subsequently deposited with a large number of voids in between allowing thus penetration of the electrolyte

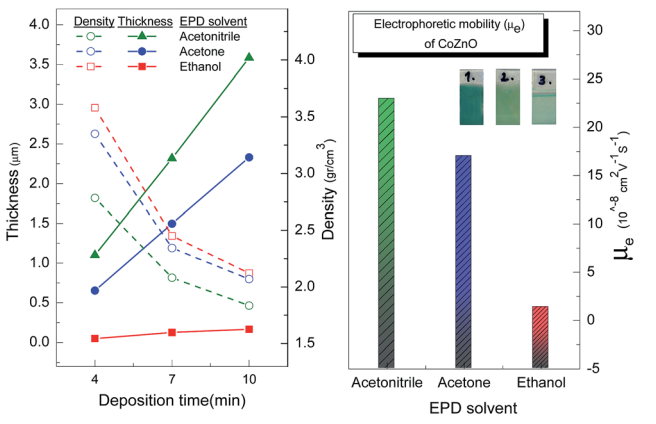

Fig. 1 (a) Effect of the organic solvent and the deposition time on the thickness and the density of the layers. (b) Influence of the organic solvent on the electrophoretic mobility of ZnO:Co particles in the suspension.

into the porous structure and accelerating charge transfer to the electrolyte. Fig. 1a shows that the densities of the layers prepared in ethanol (red line) are higher than the corresponding densities of those samples prepared in acetone (blue line) and acetonitrile (green line). In the following, the measured layer properties are discussed in terms of EPD theory, *i.e.* electrophoretic mobility and EPD deposition rate, respectively. Limitations of this approach are discussed further below.

It is well known that there exists a direct relation between deposited mass and electrophoretic mobility in the solvent under consideration (Hamaker law).[30] This relation is widely used for determination of the rate of EPD and is given by eqn (1):

$$W(t) = \int_{t_1}^{t_2} \mu E A C_s \mathrm{d}t \quad (1)$$

here, W (kg) denotes the deposited mass, μ ($m^2\ V^{-1}\ s^{-1}$) the electrophoretic mobility, E ($V\ m^{-1}$) the electric field strength, A (m^2) the electrode's surface area and C_s ($kg\ m^{-3}$) the concentration of the material in suspension. By measuring the deposited mass and using eqn (1), the electrophoretic mobility of ZnO:Co was calculated for the three different solvents. The results are shown in Fig. 1b and by the Table T3 in the ESI.† The electrophoretic mobility represents the velocity at which particles move under the influence of an applied field. This mobility depends on the viscosity and the dielectric constant of the solvent as well as the zeta (ζ) potential which serves as indication of the amount of the charge at the surface of the particles suspended in the solvent. All these parameters are considered in the Smoluchowski correlation, given by eqn (2):

$$\zeta = 3\mu\eta/(2\varepsilon_0\varepsilon_r) \quad (2)$$

here ε_0 is the permittivity of space ($8.854 \times 10^{-12}\ F\ m^{-1}$), ε_r and η ($Ns\ m^{-2}$) denote the permittivity and viscosity of the suspension medium, respectively, ζ represents the zeta potential of the particles in suspension and μ ($m^2\ V^{-1}\ s^{-1}$) expresses the electrophoretic mobility of the particles in the solvent. The electrophoretic mobility and the zeta potential of ZnO:Co particles in different solvents were accordingly calculated by eqn (1) and (2) (see Fig. 2). As shown in this figure, both the electrophoretic mobility and the zeta potential decreased slightly during increasing deposition times for all the solvents. This effect is accounted for by the progressive consumption of iodine which is required to induce the positive charge at the surface of the particles. The decreasing iodine concentration then results in a lower zeta potential and, consequently, smaller deposition rates.

As shown in Fig. 2, there is a big difference between the zeta potential of ZnO:Co particles suspended in ethanol and those dissolved in acetone and acetonitrile. This effect can be understood by the different activity of the solvents towards iodine and finally the suspended particles. Acetonitrile and acetone are polar aprotic solvents; the nitrile group in acetonitrile and the carbonyl group in acetone are proton acceptors. Polar aprotic solvents cannot participate in hydrogen bonding because of lack of O–H or N–H groups. Therefore, iodine in the

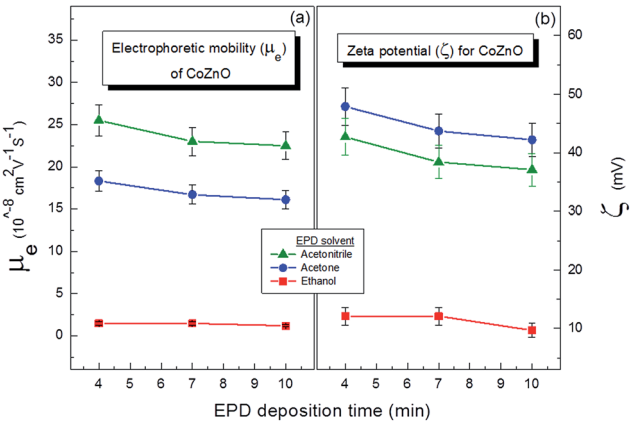

Fig. 2 (a) and (b) Effect of the organic solvent as a function of deposition time on the electrophoretic mobility and the zeta potential of the ZnO:Co particles, respectively.

solution is free and induces a positive charge at the ZnO:Co particles. In the case of ethanol, the polar-protic solvent participates in hydrogen bonding which is a powerful intermolecular force. Hydrogen bonds are more easily formed between hydrogen of the hydroxyl group and the nucleophile iodine. Therefore the concentration of iodine in the ethanol solution decreases in comparison to acetonitrile and acetone.

As a consequence, the amount of positive surface charge at the surface of the ZnO:Co particles is lowered and the horizontal movement of the particles towards the cathode is more impeded by vertical forces, *i.e.* gravitation. As a further consequence, formation of hydroiodic acid is facilitated in ethanol. The generation of acid can influence the deposition of the layers in two ways: firstly, the ZnO:Co particles are partially etched, *i.e.* they decrease in size; secondly, already deposited particles can be released from the surface if the etching process affects the interface between the FTO support and the particles. Both effects therefore contribute to an overall limited layer thickness and point beyond the assumption of a chemically inert carrier solvent assumed in our theoretical approach. Moreover, the apparent film porosity is reduced since small particles can be immobilized in a denser layer structure than larger particles. It should be noted that also for acetone formation of hydroiodic acid can be expected: due to the keton–enol tautomerism of acetone, a small fraction of –OH bonds are present in solution. It is assumed that the kinetics of this transformation is shifted towards the enol species in the presence of iodine.[31] Therefore, film properties of acetone-prepared samples, *i.e.* the density of the films, as well as electrophoretic parameters, *i.e.* the EPD deposition rate, are expected to reveal the impact of minute concentrations of hydroiodic acid, too. In fact, the data of Fig. 1 demonstrate that layer thickness and porosity as well as electrophoretic mobility are all slightly smaller than observed for acetonitrile. Only the calculated zeta potential (Fig. 2b) appears increased which has to be attributed to the larger dielectric constant of acetonitrile (compare eqn (2) and ESI Table T2†).

Optical measurements included transmission spectroscopy and normalized SPV amplitudes of ZnO:Co films prepared in

different solvents for 7 min deposition time each. The results are shown in Fig. 3a and b, respectively. The red, green and blue curves belong to samples prepared in ethanol, acetonitrile and acetone, respectively. The samples were illuminated from the front side, *i.e.* light passed through the ZnO:Co film first and only photons, not absorbed by ZnO:Co reached the FTO support. Optical transmittance spectra for ZnO:Co films prepared in different solvents for 7 min are shown in Fig. 3a.

While acetonitrile- and acetone-prepared samples show strong attenuation of the incident light, highest transmittance was achieved with samples prepared from ethanol solutions. Transmittance values near 70% therefore suggest this preparation method as suitable for photoactive supports to be discussed further below. Fig. 3a and the calculated absorption (ESI Fig. S2†) suggest an optical band gap of ZnO:Co, near 2.5 eV. A dip in the transmission curve near 2 eV and the corresponding maximum in the absorption behaviour are attributed to defect-related absorption. The nature of the defects is tentatively assigned to residual carbon from the organic suspensions and is not considered to contribute to the electrocatalytic activity. In Fig. 3b, the SPV response indicates that photo-induced excess charge carriers are separated in space.[32,33] The SPV amplitude for all the samples exhibited two response peaks (as in corresponding UV-VIS spectra): the curves increased sharply at photon energy of about 1.7–1.8 eV indicating the onset of tail states (defect levels) within the band gap of the material (see extrapolated straight lines in Fig. 3b). This onset appears related to the absorption feature near 2 eV in Fig. 3a mentioned above. The second structure, to be attributed to FTO, is not shown in Fig. 3b for clarity. It should be noted that the onset energy of electronic states extending into the band gap is always lower than the corresponding optical band gap. The results of Fig. 3b allow concluding that the use of different solvents does not significantly change the electronic defect structure of the material. X-ray diffraction patterns of ZnO:Co powder (before deposition) and ZnO:Co/FTO junctions before and after electrochemical measurements (EC) are shown in ESI Fig. S3.† GIXRD measurements were carried out at 0.2°. The results reveal a polycrystalline, highly oriented film directly after electrophoretic deposition. The dominant peaks are assigned to 101, 100 and 002 reflections. Using the Scherrer equation, average particle sizes of 24, 17 and 21 nm were calculated. After EC measurements there is a visible change in the X-ray reflection spectra. The intensity of the peaks appears reduced and crystal sizes of 18, 12 and 16 nm were obtained. In correspondence to earlier findings by Pfrommer *et al.*,[17] this change has to be attributed to a continuous transformation of the crystalline into an amorphous phase, *i.e.* the nanocrystalline powder acts as a precatalyst whose surface area continuously transforms to the final electrocatalytic material upon evolution of oxygen.[17] Correspondingly, elemental analysis by EDX proves considerable differences in the Zn:Co ratio before and after OER (see ESI Fig. S4 and Tables T4 and T5†): before electrochemical testing, the respective Zn:Co ratios for acetone-, acetonitrile- and ethanol-prepared samples were: 2.5 : 1, 2.5 : 1, and 2.6 : 1, respectively. After EC, ratios of 0.4 : 1, 0.5 : 1 and 0.1 : 1 were calculated, *i.e.* Zn is leaching into the electrolyte which relates the ZnO:Co powder to the emerging research field of metastable OER catalysts.[34,35] The variation within the latter numbers can be understood by the respective difference of the film thickness. For thin ethanol-prepared films, the Zn-poor surface region contributes more to the EDX-determined stoichiometry. For thick acetone- and acetonitrile-prepared films, more Zn-rich material is buried beneath the top-surface layer. Moreover, XPS results of the Co 2p core level (ESI Fig. S5†) suggest the presence of Co(II), *i.e.* $Co(OH)_2$, visible by pronounced shake-up signals at higher binding energies.[36] As already reported earlier,[17] a transition of Co(II) to Co(III) occurs upon OER. Therefore, the transformation of the surface region around the crystalline ZnO:Co core-nanoparticles is characterized by leaching of Zn into the electrolyte, formation of an amorphous surface layer and oxidation of Co into a higher oxidation state to achieve the final electrocatalytically active surface material. In this connection, it also appears likely that the loss of ZnO promotes formation of a three-dimensional layer structure with increased surface area and contributes thereby to the overall activity of the film. The thereby activated catalyst supports high absolute currents without deactivation during an extended period of time as demonstrated further below.

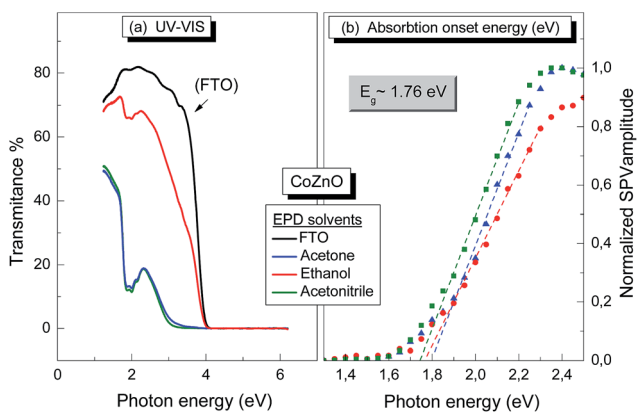

Fig. 3 Optical characterization of ZnO:Co deposited on FTO substrates (a) transmission spectra as a function of wavelength (b) normalized SPV amplitudes as a function of photon energy for ethanol (red dots), acetone (blue dots) and acetonitrile (green dots).

The electrochemical behavior of the samples was investigated by cyclic voltammetry in 1 N KOH, pH 14. Fig. 4 shows the current–voltage behavior in a three-electrode arrangement for the samples prepared in acetone (blue curve), acetonitrile (green curve) and ethanol (red curve). Corresponding two-electrode measurements as well as measurements, corrected for the uncompensated IR-drop, are shown as ESI (Fig. S7 and S11,† respectively).

Pronounced oxidation and reduction peaks around 1.4 V are visible for samples prepared in acetone and acetonitrile. For ethanol-prepared samples this reversible oxidation–reduction behavior is much less visible. In order to assess the activity of OER catalysts, steady-state Tafel plots are typically applied in the literature.[37–41] These measurements, however, require long-time current monitoring in the ultra-low current density range and appear less appropriate for samples with pronounced

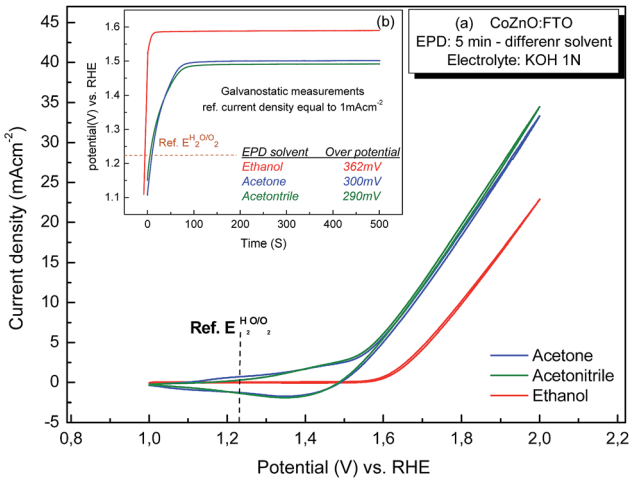

Fig. 4 (a) Current–voltage behavior of ZnO:Co prepared in different organic solvents ethanol (red line), acetone (blue line) and acetonitrile (green line) deposited on FTO substrates. (b) Galvanostatic measurements of the layers, shown as inset, correspond to a current density of 1 mA cm^{-2}. Electrolyte: KOH 1 N.

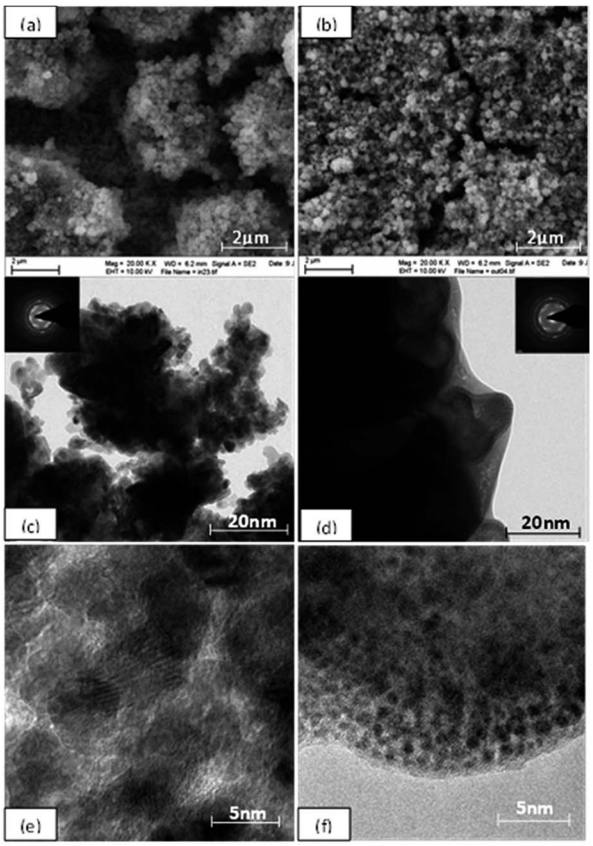

Fig. 5 Microscopy characterization of ZnO:Co morphologies after EPD using acetonitrile as solvent. (a) and (b) SEM surface view before and after electrochemistry, respectively. (c) and (d) Corresponding TEM images of ZnO:Co lamellae before and after electrochemistry, respectively. (e) and (f) Magnified TEM images of ZnO:Co lamellae before and after electrochemistry, respectively.

oxidation and reduction behavior. Instead galvanostatic determination of the potential corresponding to 1 mA cm^{-2} was used (see inset in Fig. 4) to reveal the decay of self-oxidation and to characterize the different activities. The measured potentials of 362 (ethanol), 300 (acetone) and 290 mV (acetonitrile) prove the highest activity for acetonitrile-prepared samples. Corresponding overpotentials for reported very active cobalt and cobalt-containing nickel-iron oxides range between about 280 and about 400 mV demonstrating the high activity of the activated ZnO:Co catalyst presented here.[37–41] Using differential electrochemical mass spectroscopy it is finally proven that commencing current densities are related to evolution of oxygen (ESI Fig. S8†). Considering the observed relation of higher film porosity (Fig. 1a) and higher OER activity (Fig. 4) we conclude that the size of the active surface area is the most crucial distinguishing film property that makes acetonitrile-(acetone-) prepared ZnO:Co films more favorable. This property, in turn, is directly related to the difference in electrophoretic mobility of the ZnO:Co particles in the respective organic solvents (Fig. 1b).

SEM and TEM images for ZnO:Co, deposited from acetonitrile- and ethanol-containing suspensions are shown in Fig. 5 and 6. The corresponding analysis for acetone-prepared samples is presented as ESI Fig. S9.† Left-row images depict the materials structure before electrochemical operation. Right-row images show the corresponding analyses after electrochemistry. On the larger scale of the SEM images, the least changes are visible with samples deposited from ethanol (Fig. 6a and b). Due to the higher porosity and therefore higher active surface area, those changes are more pronounced for samples prepared from acetonitrile and acetone (Fig. 5 and S9a and b,† respectively). Closer inspection by TEM analysis of small lamellae (and selected area electron diffraction images) reveals the commencing transition to an amorphous phase by exposure to the electrolyte under anodic potential (compare the respective images c through f).

This transition is almost completed with ethanol-prepared samples while with acetonitrile and acetone prepared samples, distinguishable diffraction patterns can still be observed. The pronounced amorphous state of ZnO:Co films, prepared from ethanol solutions, also explains the observed highest decrease of Zn concentrations upon evolution of oxygen discussed above: the amorphous phase obviously facilitates dissolution of Zn by formation of zinc hydroxide.

The stability behavior of the respective ZnO:Co films in 1 N KOH, pH 14, was measured over a period of 24 hours and is shown in Fig. 7a. Potentials were adjusted such that current densities were close to 4 mA cm^{-2} in the beginning. For clarity, the curves in Fig. 7a are presented after applying a positive small current density shift (between 0.5 and 1 mA cm^{-2}). For all samples a current decrease by about 10% was observed. Cross-check analysis of the behavior of bare FTO in 1 N KOH, however, proved pronounced instability of the support (Fig. 7a). In order to achieve more insight into the long-term behavior, an ethanol-prepared sample was additionally tested over 72 hours (Fig. 7b). After that time, the electrolyte was renewed as indicated by an

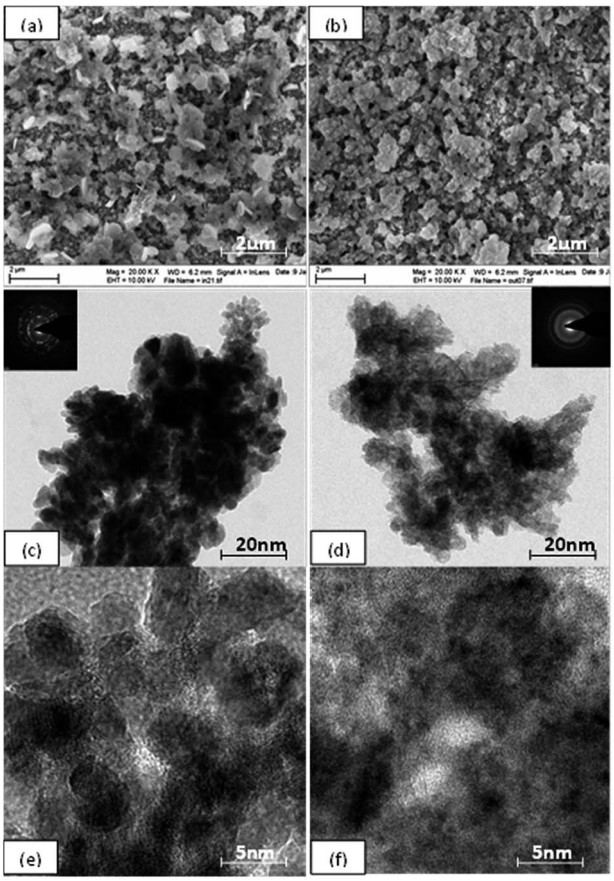

Fig. 6 Microscopy characterization of ZnO:Co morphologies after EPD using ethanol as solvent. (a) and (b) SEM surface view before and after electrochemistry, respectively. (c) and (d) Corresponding TEM images of ZnO:Co lamellae before and after electrochemistry, respectively. (e) and (f) Magnified TEM images of ZnO:Co lamellae before and after electrochemistry, respectively.

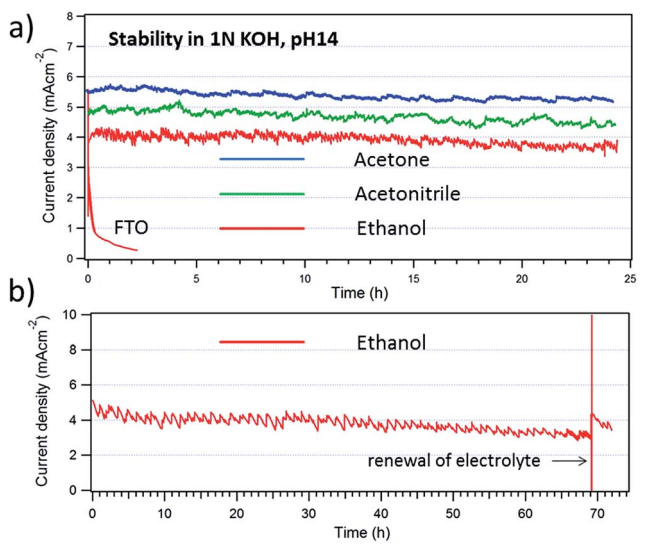

Fig. 7 Stability assessment of ZnO:Co, prepared from ethanol-containing suspensions, at pH 14. For comparison, the rapid degradation of a bare FTO substrate is indicated.

arrow. It can be seen that the renewed electrolyte permits partial compensation of the current decrease. Initial high values, however, are not reached anymore. This finding can be attributed either to a loss in activity of the catalytic material or, more likely, to structural flaws within the film which lead to progressive degradation of the FTO support.

It is finally shown that the enhanced optical transparency of ethanol-prepared samples can be successfully employed for solar-cell biased direct splitting of water. The schematic of the setup with a triple-junction solar cell (amorphous silicon) is depicted in Fig. 8. The ZnO:Co/FTO top-junction covered the 1 cm^2 photoactive area of the solar cell completely. For visibility of the photoactive area in the top-view of Fig. 8, the size of the ZnO:Co containing area was reduced. Dashed lines in Fig. 8 indicate the charge flow along the employed external wiring.

Corresponding photocurrent–voltage curves, measured with Pt-counter electrode, are presented in Fig. 9. Due to the only small light attenuation by ZnO:Co prepared from ethanol, about 70% of the short circuit photocurrent can be exploited for light-driven evolution of oxygen. The solar-to-hydrogen (STH)[42] efficiency thereby amounts to:

$$\eta = \frac{1.23\ \mathrm{V} \times J_0}{A \times 100\ \mathrm{mW\ cm^{-2}}} = 5\%. \quad (3)$$

Here, J_0 denotes the short-circuit photocurrent density and A the illuminated area of 1 cm^2. The illumination intensity was 100 mW cm^{-2} corresponding approximately to AM 1.5 conditions. Corresponding measurements with acetonitrile- and acetone-prepared samples are shown as ESI (Fig. S10†) and exhibit much lower efficiencies due to large light absorption in the thick electrocatalytic layers.

It is worth noting that the modular architecture presented here allows a simple exchange of the ZnO:Co/FTO

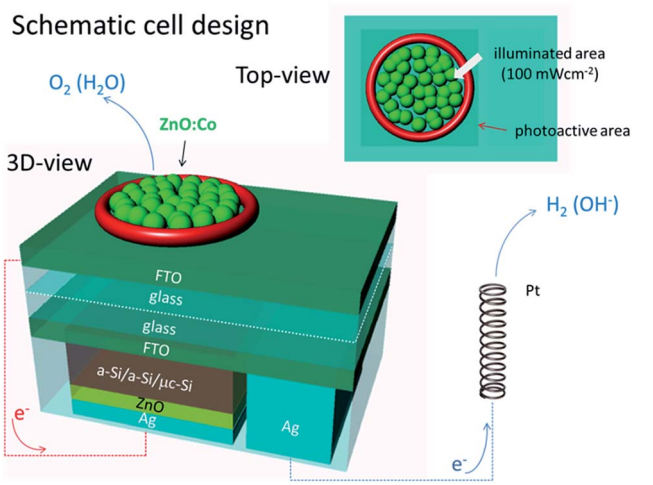

Fig. 8 Schematic setup of the combined junctions, an amorphous/microcrystalline silicon solar cell (bottom) and a ZnO:Co/FTO heterojunction (top). The white dashed line in the 3D-schematic indicates where the top ZnO:Co/FTO electrode can be lifted off. In the top-view, the O-ring is depicted in decreased size in order to stress the photoactive area beneath.

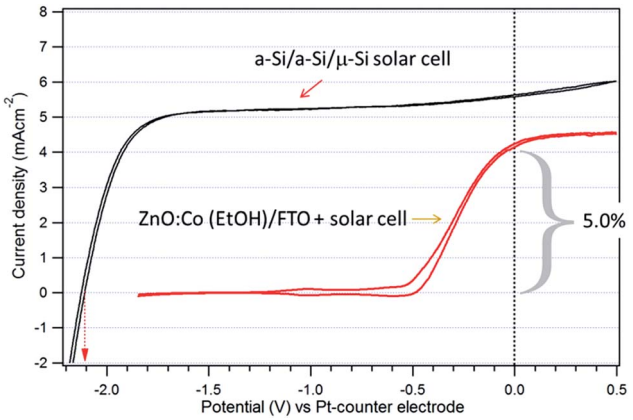

Fig. 9 Photocurrent–voltage behavior of ZnO:Co/FTO prepared from ethanol suspensions. The electrocatalytic layer was fixed to the photoactive front-side of the triple-junction silicon solar cell (compare Fig. 8). Short-circuit photocurrent densities of about 4.2 mA cm^{-2} result in an efficiency of 5% for direct photo-assisted water splitting.

electrocatalyst once its activity has fallen below a minimum threshold value.

Considering the use of low-cost, earth-abundant electrocatalysts, this approach appears to be an attractive alternative to designs where the catalysts are permanently fixed to the photoactive supports. In the latter case, any degradation of the electrocatalytic layer will affect the efficiency of the entire structure. Moreover, with further advancements in solar cell development, the STH efficiency seamlessly increases as well. Hence, the concept of low-cost PV coupled to low-cost electrolyzers in the suggested stacking configuration represents an attractive approach for addressing the huge challenge of long-term stability of photoelectrocatalytic devices.

Conclusions

We presented a systematic study on the correlation of ZnO:Co thin film deposition rates and film structure properties with the electrophoretic mobility and the zeta potential in different organic solvents. The functionalization of ZnO:Co particles on FTO supports was shown to depend on the size of the active surface area. Upon variation of the organic solvents, used for electrophoretic deposition, it was shown that the use of acetonitrile results in a surface morphology with highest active surface area. Consequently, the overpotential for the evolution of oxygen observed at 1 mA cm^{-2} could be reduced from 360 mV to 290 mV RHE. Combining ZnO:Co electrocatalysts and low-cost photovoltaic triple-junctions, we have successfully demonstrated a proof-of-concept for an efficient modular architecture for generation of solar hydrogen (up to 5% STH and long-term stability on the scale of several days).

Acknowledgements

We are grateful for the support given by S. Kirner, R. Schlatmann, P. Bogdanoff and R. van de Krol. We gratefully acknowledge the financial supports provided by the BMBF excellence cluster project "Light2Hydrogen" (No. 03IS2071F) and by the Deutsche Forschungsgemeinschaft (DFG) project (No. SCHE 533/3-1) in the frame of the priority program SPP 1613-"Solar-H_2".

References

1 M. W. Kanan and D. G. Nocera, *Science*, 2008, **321**, 1072.
2 Y. Surendranath, M. Dinca and D. G. Nocera, *J. Am. Chem. Soc.*, 2009, **131**, 2615.
3 N. D. Morris, M. Suzuki and T. E. Mallouk, *J. Phys. Chem. A*, 2004, **108**, 9115.
4 P. G. Hoertz, Y. Kim, W. J. Youngblood and T. E. Mallouk, *J. Phys. Chem. B*, 2007, **111**, 6845.
5 W. J. Youngblood, S.-H. A. Lee, Y. Kobayashi, E. A. Hernandez-Pagan, P. G. Hoertz, T. A. Moore, A. L. Moore, D. Gust and T. E. Mallouk, *J. Am. Chem. Soc.*, 2009, **131**, 926.
6 B. O'Regan and M. Gräetzel, *Nature*, 1991, **353**, 737.
7 H. Dau, C. Limberg, T. Reier, M. Risch, S. Roggan and P. Strasser, *ChemCatChem*, 2010, **2**, 724.
8 H. Dau and I. Zaharieva, *Acc. Chem. Res.*, 2009, **42**, 1861.
9 H. Inoue, T. Shimada, Y. Kou, Y. Nabetani, D. Masui, S. Takagi and H. Tachibana, *ChemSusChem*, 2011, **4**, 173.
10 F. F. Abdi, L. Han, A. H. M. Smets, M. Zeman, B. Dam and R. van de Krol, *Nat. Commun.*, 2013, **4**, 2195.
11 S. W. Warren, K. Voïtchovsky, H. Dotan, C. M. Leroy, M. Cornuz, F. Stellacci, C. Hébert, A. Rothschild and M. Grätzel, *Nat. Mater.*, 2013, **12**, 842–849.
12 M. J. Kenney, M. Gong, Y. Li, J. Z. Wu, J. Feng, M. Lanza and H. Dai, *Science*, 2013, **342**, 836.
13 S. Trasatti and G. Lodi, *Electrodes of Conductive Metallic Oxides*, Elsevier, Amsterdam, 1981, pp. 521–626.
14 M. Risch, A. Grimaud, K. J. May, K. A. Stoerzinger, T. J. Chen, A. N. Mansour and Y. Shao-Horn, *J. Phys. Chem. C*, 2013, **117**, 8628.
15 A. Grimaud, C. E. Carlton, M. Risch, W. T. Hong, K. J. May and Y. Shao-Horn, *J. Phys. Chem. C*, 2014, **117**, 25926–25932.
16 S. W. Lee, C. Carlton, M. Risch, Y. Surendranath, S. Chen, S. Furutsuki, A. Yamada, D. G. Nocera and Y. Shao-Horn, *J. Am. Chem. Soc.*, 2012, **134**, 16959–16962.
17 J. Pfrommer, M. Lublow, A. Azapira, C. Göbel, M. Lücke, A. Steigert, M. Pogrzeba, P. W. Menezes, A. Fischer, T. Schedel-Niedrig and M. Driess, *Angew. Chem., Int. Ed.*, 2014, **53**, 5183.
18 D. M. Jang, I. H. Kwak, E. L. Kwon, C. S. Jung, H. S. Im, K. Park and J. Park, *J. Phys. Chem. C*, 2015, **119**, 1921.
19 L. Besra and M. Liu, *Mater. Sci.*, 2007, **52**, 1.
20 M. Ammam, *RSC Adv.*, 2014, **2**, 7633.
21 F. Begona and M. Rodrigo, *J. Eur. Ceram. Soc.*, 2010, **30**, 1069.
22 I. Corni, M. P. Ryan and A. R. Boccaccini, *J. Eur. Ceram. Soc.*, 2008, **28**, 1353.
23 O. van der Biest and L. J. Vandeperre, *Annu. Rev. Mater. Sci.*, 1999, **29**, 327.
24 S. Polarz, A. V. Orlov, M. W. E. van den Berg and M. Driess, *Angew. Chem., Int. Ed.*, 2005, **44**, 7892.

25 M. L. Tong, S. L. Zheng, J. X. Shi, Y. X. Tong, H. K. Lee and X. M. Chen, *J. Chem. Soc., Dalton Trans.*, 2002, 1727.
26 S. Kirner, S. Neubert and C. Schulz, *Jpn. J. Appl. Phys.*, 2015, **54**, 08KB03.
27 L. Kronik and Y. Shapira, *Surf. Sci. Rep.*, 1999, **37**, 1–206.
28 S. Ashton, *Design, construction and research application of a Differential Electrochemical Mass Spectrometer (DEMS)*, Springer Theses, 2012, ISBN 978-3-642-30550-4.
29 P. Bogdanoff and N. Alonso-Vante, *J. Electroanal. Chem.*, 1994, **379**, 415.
30 H. C. Hamaker, *Trans. Faraday Soc.*, 1940, **36**, 279.
31 K. Peter, C. Vollhardt and N. E. Schore, *Organische Chemie*, Wiley-VCH Verlag GmbH & Co. KGaA, Weinheim, 2005, p. 4, Auflage, H. Butenschön, ISBN 3-527-31380-X, S. 921-922.
32 A. Juma, J. Kavalakkatt, P. Pistor, B. Latzel, K. Schwarzburg and T. Dittrich, *Phys. Status Solidi A*, 2012, **209**, 663.
33 L. Macor, M. Gervaldo, F. Fungo, L. Otero, T. Dittrich, C. Y. Lin, L. C. Chi, F.-C. Fang, S.-W. Lii, C.-H. Tsai and C.-C. Wu, *RSC Adv.*, 2012, **2**, 4869.
34 T. Binninger, R. Mohamed, K. Waltar, E. Fabbri, P. Levecque, R. Kötz and T. J. Schmidt, *Sci. Rep.*, 2015, **5**, 12167.
35 M. García-Mota, M. Bajdich, V. Viswanathan, A. Vojvodic, A. T. Bell and J. K. Norskov, *J. Phys. Chem. C*, 2012, **116**, 21077.
36 M. C. Biesinger, B. P. Paynec, A. P. Grosvenord, L. M. Laua, A. R. Gersonb and R. St. C. Smart, *Appl. Surf. Sci.*, 2011, **257**, 2717.
37 L. Trotochaud, J. K. Ranney, K. N. Williams and S. W. Boettcher, *J. Am. Chem. Soc.*, 2012, **134**, 17253.
38 R. D. L. Smith, M. S. Prévot, R. D. Fagan, Z. Zhang, P. A. Sedach, M. K. J. Siu, S. Trudel and C. P. Berlinguette, *Science*, 2013, **30**, 60.
39 J. B. Gerken, J. G. McAlpin, J. Y. C. Chen, M. L. Rigsby, W. H. Casey, R. D. Britt and S. S. Stahl, *J. Am. Chem. Soc.*, 2011, **133**, 14431.
40 R. D. L. Smith, M. S. Prévot, R. D. Fagan, S. Trudel and C. P. Berlinguette, *J. Am. Chem. Soc.*, 2013, **135**, 11580.
41 M.-R. Gao, Y.-F. Xu, J. Jiang, Y.-R. Zheng and S.-H. Yu, *J. Am. Chem. Soc.*, 2012, **134**, 2930.
42 H. Dotan, N. Mathews, T. Hisatomi, M. Grätzel and A. Rothschild, *J. Phys. Chem. Lett.*, 2014, **5**, 3330.

